

# Model-based Asynchronous Hyperparameter Optimization

Louis C. Tiao<sup>1</sup> Aaron Klein<sup>2</sup> Cédric Archambeau<sup>2</sup> Matthias Seeger<sup>2</sup>

## Abstract

We introduce a model-based asynchronous multi-fidelity hyperparameter optimization (HPO) method, combining strengths of asynchronous Hyperband (Li et al., 2018) and Gaussian process-based Bayesian optimization (Swersky et al., 2013). Our method obtains substantial speed-ups in wall-clock time over, both, synchronous and asynchronous Hyperband, as well as a prior model-based extension of the former (Falkner et al., 2018). Candidate hyperparameters to evaluate are selected by a novel jointly dependent Gaussian process-based surrogate model over all resource levels, allowing evaluations at one level to be informed by evaluations gathered at all others. We benchmark several covariance functions and conduct extensive experiments on hyperparameter tuning for multi-layer perceptrons on tabular data, convolutional networks on image classification, and recurrent networks on language modelling, demonstrating the benefits of our approach.

## 1. Introduction

The goal of hyperparameter optimization (HPO) is to automate the process of finding the best hyperparameters  $\mathbf{x}_* \in \arg \min_{\mathbf{x} \in \mathcal{X}} f(\mathbf{x})$  for a machine learning algorithm that minimizes a validation loss  $f(\mathbf{x})$ , which we assume to be observed through noise:

$$y_i = f(\mathbf{x}_i) + \epsilon_i, \quad \epsilon_i \stackrel{\text{iid}}{\sim} \mathcal{N}(0, \sigma^2), \quad i = 1, \dots, n.$$

Bayesian optimization (BO) (Jones et al., 1998; Shahriari et al., 2016) is a model-based approach that provides an effective framework for HPO. It constructs a probabilistic surrogate model of the loss function  $p(f | \mathcal{D})$  based on previous evaluations  $\mathcal{D} = \{(\mathbf{x}_i, y_i)\}_{i=1}^n$ . Searching the global minimum of  $f$  is then driven by trading off exploration in

<sup>1</sup>University of Sydney, Australia <sup>2</sup>Amazon Berlin, Germany. Correspondence to: Louis C. Tiao <louis.tiao@sydney.edu.au>, Aaron Klein <kleiaaro@amazon.com>, Matthias Seeger <matthis@amazon.com>.

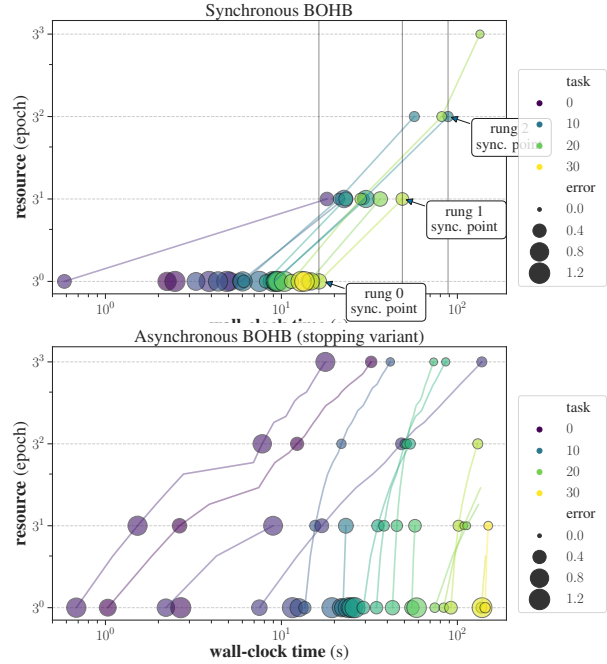


Figure 1. The initial 150s of synchronous BOHB (top) the proposed asynchronous BOHB stopping variant (bottom). Each line corresponds to a hyperparameter configuration, representing the points in time at which training epochs were completed, with markers denoting each of the rungs it has reached. The hue signifies the order in which configuration were proposed and queued for evaluation. The size of each marker is proportional to the validation error observed at the rung. Asynchronous BOHB is able to evaluate more configuration in the given time budget since workers do not idle at synchronization points. See Section 2 for further details.

regions where our model is uncertain and exploitation in regions where the global optimum is assumed to be located.

The evaluation of each set of hyperparameters requires training from scratch. This can render BO expensive as, for example in the context of deep neural networks, the entire training can take hours or even days. The overall optimization process can be accelerated by stopping the training of unpromising hyperparameter configurations early, while still using the corresponding evaluations as low-fidelity approximations of  $f$  (Swersky et al., 2014b; Domhan et al., 2015; Klein et al., 2017b). Additionally, evaluations of  $f$  can be distributed across parallel compute resources to further reduce the wall-clock time required for finding a good solution.

Successive halving (SH) (Jamieson & Talwalkar, 2016) considers  $n$  randomly drawn hyperparameter configurations, which are first evaluated based on some given initial resource  $r_{\min}$ . Next, only the best  $n/\eta$  configurations are continued with a higher resource level of  $r_{\min}\eta$ . This process is repeated until a maximum resource level  $r_{\max}$  is reached. Each iteration of SH is called a *rung*.

Hyperband (HB) (Li et al., 2017) extends SH by an outer loop, where instances of SH, called *brackets*, are run with a variable number of initial configurations  $n$  and initial resource level  $r_{\min}$ , such that each bracket roughly consumes the same amount of total resources. This simple, model-free strategy can outperform BO in the first phase of the optimization process, and is trivial to parallelize across different workers (Li et al., 2017). Falkner et al. (2018) introduced BOHB which combines the efficient anytime performance of HB with a probabilistic model to stir the search. However, in its standard form, both HB and BOHB are *synchronous*, in a sense that the evaluation of all configurations in a given rung have to finish before any of the configurations can be promoted to the next rung.

This synchronous scheduling can be problematic when the evaluation of some configurations take longer than others (so-called *stragglers*), which leads to delayed promotions of high-performing configurations to the upper rungs (see Figure 1 for an illustration).

### 1.1. Contributions

In this work, we combine multi-fidelity BO with an asynchronous parallel scheduling, inspired by asynchronous HB (Li et al., 2018). More specifically, we make the following contributions:

- We introduce a new model-based extension of asynchronous HB that can handle multi-fidelity evaluations in a principled way. The new BO method simultaneously reasons across rungs and asynchronously across workers. The underlying surrogate model is a joint Gaussian process (GP) similar to the one used by Swersky et al. (2013; 2014a) but without requiring any further approximations.
- We analyse and compare two recently proposed asynchronous variants of SH in the context of model-based HB. Furthermore, we also propose and compare several kernel functions to model the loss across different resource levels.
- On a range of neural network benchmarks, we show that, especially if they are extremely expensive to evaluate, our proposed method is more efficient in terms of wall-clock time than other state-of-the-art HPO strategies that work either synchronously or rely on random

sampling.

Next, we relate our work to approaches recently published in the literature. In Section 2, we review synchronous SH and HB, as well as two asynchronous extensions. Our novel method is presented in Section 3. We present empirical evaluations for the HPO of various deep neural network architectures in Section 4, and finish with conclusions and future work in Section 5.

### 1.2. Related Work

There is a range of literature on Gaussian process (GP) based BO that exploits fidelities of the objective function to speed-up the optimization process (Kennedy & O’Hagan, 2000; Klein et al., 2017a; Poloczek et al., 2018; Cutajar et al., 2018), see also Section 1.4.3 in (Feurer & Hutter, 2019). Swersky et al. (2013) introduced a joint GP model across configurations and tasks which allows BO to evaluate most of the configurations on a cheaper auxiliary task and only evaluate few configurations on the expensive main task. However, their multi-task GP is not able to incorporate prior knowledge on how the performance changes across these discrete fidelities. To reason across training dataset subsets, Klein et al. (2017a) presented a continuous multi-fidelity BO method, which gets as additional input the training dataset size. Their GP model consists of a dot product kernel which allows to incorporate prior assumptions about the objective function by specifying sensible basis functions. However, their BO strategy relies on a sophisticated and expensive information theoretic acquisition function.

Synchronous HB has already been combined with BO by Falkner et al. (2018), which, similar to Bergstra et al. (2011), maintains a kernel density estimator (KDE) to model the distribution of good and bad configurations. This approach, dubbed BOHB, retains the early speed-ups of HB, while converging faster later on. However, compared to our joint model, they fit a model at each resource level independently, which hinders the transfer of knowledge across rungs. Furthermore, the KDE model is not able to fantasize the outcome of pending evaluations, making it impractical for the asynchronous setting. Another model-based extension of synchronous HB was proposed by Valkov et al. (2018), with the specific goal to warm-start HPO. Again, it does not consider asynchronous scheduling or decision making based on pending feedback. Our method is free of synchronization points, thus consuming the available computation budget most efficiently at any point in time.

Also relevant to our work is the “freeze-thaw” setup by Swersky et al. (2014a), which allows for asynchronous parallel evaluations, yet whose scheduling is quite different from asynchronous HB and has not shown any performance for the HPO of deep neural networks. Instead of just modelling

the performance at certain rung levels, their GP model takes the entire learning curve into account. In order to reduce the cubic complexity of the GP, Swersky et al. (2014a) decompose the GP and model, conditioned on the asymptotic performance, learning curves independently.

Previous work on asynchronous BO has demonstrated performance gains over synchronous BO methods (Alvin et al., 2019; Kandasamy et al., 2018). However, this work did not take multiple fidelities of the objective function into account.

## 2. Synchronous and Asynchronous Multi-Fidelity Scheduling

In the context of this work, *multi-fidelity* HPO considers an objective  $f(\mathbf{x}, r)$ , indexed by the *resource level*  $r \in \{r_{\min}, \dots, r_{\max}\}$ . The target function of interest is  $f(\mathbf{x}) = f(\mathbf{x}, r_{\max})$ , while evaluations of  $f(\mathbf{x}, r)$  for  $r < r_{\max}$  are low-cost low-fidelity evaluations that may be correlated with  $f(\mathbf{x})$  and therefore help guide the search. In our work, we consider the number of training epochs (*i.e.*, full sweeps over the data) as the resource  $r$ , though other choices can be sensible as well (*e.g.*, training subset ratio).

Parallel multi-fidelity HPO methods, such as HB or BOHB, explore the space of hyperparameters by making two kinds of complementary decisions: *choosing* configurations to evaluate and *scheduling* their evaluations, which includes resource allocation. Scheduling decisions are constrained to certain resource *rungs*, chosen according to the Successive Halving principle (Jamieson & Talwalkar, 2016). Let us denote the halving constant by  $\eta \in \{2, 3, 4\}$ , and let  $r_{\max}$  and  $r_{\min}$  be the maximum and minimum resource level for an evaluation, respectively. For notational simplicity, we assume that  $r_{\max}/r_{\min} = \eta^K$ . The full set of rungs is  $\mathcal{R} = \{r_{\min}\eta^k \mid k = 0, \dots, K\}$ . Then, *brackets* are (ordered) subsets  $B_s = \{r_{\min}\eta^{k+s} \mid k = 0, \dots, K-s\} \subseteq \mathcal{R}$ , where  $s = 0, \dots, K$ . Here,  $B_0$  contains all rungs,  $|B_0| = K+1$ , while  $B_K = \{r_{\max}\}$ . In the sequel, the term “rung” will be overloaded to both mean the resource level at which stop/go decisions are made, and the list of configs which reached this level, along with the metric values attained there.

We distinguish between *synchronous* and *asynchronous* scheduling. Synchronous scheduling is detailed in Li et al. (2017); Falkner et al. (2018). In a nutshell, each rung of each bracket has an *a priori* fixed size (*i.e.*, number of slots for configs evaluated until the rung level), the size ratio between successive rungs being  $\eta^{-1}$ . Hyperparameter configurations promoted to a rung are evaluated until the corresponding resource level, making use of parallel computation. Once all of them finish, the  $\eta^{-1}$  fraction of top performing configurations are promoted to the next rung while the others are terminated. In other words, there are synchronization

points at all but the highest rung. Also, a rung has to be populated entirely before any configuration can be promoted to the next one. In an outer loop, the algorithm cycles over brackets  $s = 0, \dots, K$  periodically until the total budget is spent. Note that synchronous scheduling requires the ability to pause-and-resume training. If this is not supported, one can also start training from scratch for each promoted configuration.

We considered two different asynchronous generalizations of HB. We first introduce common concepts. The evaluation of a configuration is driven by one or more *tasks*. A task is a computational workload to be performed by a worker. For any configuration, its bracket index  $s \in \{0, \dots, K\}$  determines the rung levels  $B_s$  at which scheduling decisions are made. The bracket index  $s$  is sampled at random according to some distribution  $P(s)$ . For example,  $P(s)$  is proportional to bracket sizes in synchronous Hyperband (Li et al., 2017). Further details about our bracket sampling strategy are included in Appendix A.1. A task evaluates a configuration  $\mathbf{x}$  until some rung  $r \in B_s$  and records the metric  $y$  observed at  $(\mathbf{x}, r)$ . Next, as long as  $r < r_{\max}$ , a *binary decision* is made for this configuration: if its metric is in the top  $\eta^{-1}$  fraction of values recorded there, “CONTINUE” evaluating until the next rung; otherwise “STOP”. The two variants differ in when such decisions are made, the meaning of “STOP”, and what happens if fewer than  $\eta$  metrics are recorded at a rung.

**Stopping variant.** In the *stopping variant*, as implemented in Ray Tune (Liaw et al., 2018), an evaluation is driven by a *single* task. Decisions are made once the task reaches a rung, and “STOP” means termination, freeing the worker to start a task to evaluate a new configuration. Furthermore, if there are fewer than  $\eta$  metrics recorded at a rung, then the evaluation is automatically allowed to continue.

**Promotion variant.** In the *promotion variant*, also called ASHA (Li et al., 2018), an evaluation is generally driven by *multiple* tasks. A “STOP” decision results in the configuration being *paused* at its current rung, but it may potentially be *promoted* (*i.e.*, continued to the following rung) later on.<sup>1</sup> Further, with fewer than  $\eta$  metrics recorded at a rung, the outcome is automatically “STOP” (*i.e.*, pause). Moreover, decisions are made whenever a worker is free. After sampling the bracket  $s$ , we scan the rungs  $r \in B_s$  in descending order and run a task to promote the first paused configuration whose decision results in “CONTINUE”. When no such paused configuration exists, we start a task to evaluate a new configuration from scratch. Different to stopping, the promotion variant needs pause-and-resume training.

<sup>1</sup> In ASHA (Li et al., 2018), tasks only ever run a configuration until the next rung, where it is paused. In our implementation, a task may continue at a rung if the promotion decision is positive, which implies less task-switching.

Synchronous scheduling makes less efficient use of parallel computation than its asynchronous counterparts. While configurations in the same rung share a common resource level (e.g., number of training epochs), their compute time can vary substantially, for example, if we search over hyperparameters that control the size of the neural network. In particular, at higher rungs, where fewer configurations need to run for longer, some workers may just be idle at a synchronization point. Such points do not exist in the asynchronous case. Finally, the rung levels have fixed sizes, which have to be filled before any configuration can be promoted, while promotions to large resource levels, up to  $r_{\max}$ , can happen earlier with asynchronous scheduling. However, the latter risks promoting mediocre configurations simply because they were selected earlier. See Figure 1 for an illustration of these differences.

The stopping and promotion variants can exhibit rather different behavior. At least initially, the stopping variant gives most configurations the benefit of doubt, while promotion is more conservative, pausing evaluations until they can be compared against a sufficient number of others. Both variants can exhibit a marked skew away from the rung size ratios in synchronous HB. Denote by  $c_s(r)$  the (time-variant) number of configurations in bracket  $s$  that were stopped in rung  $r \in B_s$ . In synchronous HB, by construction, we are guaranteed  $c_s(r\eta)/c_s(r) = 1/\eta$  for all  $r \in B_s \setminus \{r_{\max}\}$ , while in asynchronous HB or BOHB, we often see substantial skews  $c_s(r\eta)/c_s(r) \gg 1/\eta$ , in particular for  $s = 0$  and  $r = r_{\min}$ . We describe an approach to ameliorate this skew in Appendix A.2.

### 3. Model-based Asynchronous Hyperparameter Optimization

The configurations to be evaluated in HB are drawn at random from the configuration space. Motivated by the fact that in standard sequential settings, Gaussian process (GP) based BO tends to outperform random search (Shahriari et al., 2016), we aim to equip asynchronous HB with decisions based on a *GP surrogate model*. Recall that  $\mathbf{x}$  denotes the hyperparameter configuration,  $r$  the resource level (see Section 2). Following a range of prior work on non-parallel multi-fidelity BO (Swersky et al., 2013; Klein et al., 2017a; Poloczek et al., 2018; Swersky et al., 2014a), we place a GP prior over  $f(\mathbf{x}, r)$  to jointly model not only the auto-correlation within each fidelity, but also the cross-correlations between fidelities,

$$f(\mathbf{x}, r) \sim \mathcal{GP}(\mu(\mathbf{x}, r), k((\mathbf{x}, r), (\mathbf{x}', r'))).$$

Our novel GP surrogate model is an extension of Swersky et al. (2014a) that, unlike previous work by Falkner et al. (2018), explicitly captures correlations across all fidelities instead of having a separate independent model for each

fidelity.

Since multiple configurations are evaluated in parallel, we have to deal with *pending* evaluations when proposing new configurations to be evaluated. We do so by *fantasizing* their outcomes, as detailed in (Snoek et al., 2012). In a nutshell, we marginalize the acquisition function over the GP posterior predictive of evaluation outcomes for pending configurations. In practice, we approximate this by averaging the acquisition function over sampled function values. It is worth noting that as long as kernel hyperparameters remain constant, fantasizing comes almost for free. For GP regression, the posterior covariance matrix does not depend on the function values (only on the inputs), which means that fantasizing does not require additional cubic-complexity computations. Kernel parameters may be updated with empirical Bayes or Markov chain Monte Carlo.

How do pending evaluations and fantasizing generalize to the asynchronous case? The relevant covariates are now the pairs  $(\mathbf{x}, r)$ . As a task for  $\mathbf{x}$  runs down a bracket  $s$ , it emits target values at  $r \in B_s$  (unless stopped). The following logic is task-local and ensures that each labeled covariate was previously pending. If a task to evaluate  $\mathbf{x}$  is started in bracket  $s$ , we register a pending evaluation for  $(\mathbf{x}, r_{\min}\eta^s)$ . Once it reaches the next rung  $r \in B_s$ , we convert the *pending* to a *labeled* evaluation  $(\mathbf{x}, r)$ . Then, as detailed above, we make a stopping decision. If the configuration survives, we register  $(\mathbf{x}, r\eta)$  as *pending*, as  $r\eta$  is the next rung it will reach. Details about how posterior distributions over both labeled and labeled plus fantasized evaluations are represented, are given in Appendix B.1. Suffice it to say, all linear algebra computations are delayed until the posterior is needed for the next decision.

#### 3.1. Exponential Decay Surrogate Model

The model proposed by Swersky et al. (2014a) is based on the assumption  $f(\mathbf{x}, r) = f(\mathbf{x}) + e^{-\lambda r}$ , where  $\lambda \sim p(\lambda)$  is drawn from a Gamma prior, and the asymptote  $f(\mathbf{x})$  (i.e.,  $f(\mathbf{x}, r)$  as  $r \rightarrow \infty$ ) from a GP prior. They end up using a zero-mean GP prior with kernel function  $k((\mathbf{x}, r), (\mathbf{x}', r')) = k_{\mathcal{X}}(\mathbf{x}, \mathbf{x}') + k_{\mathcal{R}}(r, r')$  and

$$k_{\mathcal{R}}(r, r') := \int_0^\infty e^{-\lambda r} e^{-\lambda r'} p(\lambda) d\lambda = \kappa(r + r'),$$

$$\kappa(u) := \frac{\beta^\alpha}{(u + \beta)^\alpha}, \quad \alpha, \beta > 0.$$

This proposal has several shortcomings. First,  $f(\mathbf{x}, r) \rightarrow f(\mathbf{x}) + 1$  as  $r \rightarrow 0$ , independent of what metric is used. Second, the random function  $e^{-\lambda r}$  assumption implies a non-zero mean function, and a kernel taking this into account. A better assumption would be  $f(\mathbf{x}, r) = f(\mathbf{x}) + \gamma e^{-\lambda r}$ ,  $\gamma > 0$ , which implies a mean function  $\mu(\mathbf{x}, r) = \mu_{\mathcal{X}}(\mathbf{x}) + \gamma \kappa(r)$

and a covariance function

$$k((\mathbf{x}, r), (\mathbf{x}', r')) = k_{\mathcal{X}}(\mathbf{x}, \mathbf{x}') + \gamma^2 \tilde{k}_{\mathcal{R}}(r, r'), \quad (1)$$

$$\tilde{k}_{\mathcal{R}}(r, r') := \kappa(r + r') - \kappa(r)\kappa(r').$$

One advantage of this additive model structure is that an implied conditional independence relation can be exploited in order to speed up inference computations (Swersky et al., 2014a). However, this model implies  $f(\mathbf{x}, r) = f(\mathbf{x}) + \gamma$  as  $r \rightarrow 0$ : the metric for no training at all depends on  $\mathbf{x}$  in the same way as the asymptote. A more sensible assumption would be  $f(\mathbf{x}, r) = \gamma$  as  $r \rightarrow 0$ , since without training, predictions should be random (e.g.,  $\gamma = \frac{1}{2}$  for binary classification). We present a novel surrogate model which can incorporate this assumption. It is based on

$$f(\mathbf{x}, r) = \gamma e^{-\lambda r} + f(\mathbf{x}) (1 - \delta e^{-\lambda r}), \quad \delta \in [0, 1]. \quad (2)$$

Some algebra (provided in Appendix B.2) gives

$$\mu(\mathbf{x}, r) = \gamma \kappa(r) + \mu_{\mathcal{X}}(\mathbf{x})(1 - \delta \kappa(r)),$$

$$k((\mathbf{x}, r), (\mathbf{x}', r')) = (\gamma - \delta \mu_{\mathcal{X}}(\mathbf{x})) \tilde{k}_{\mathcal{R}}(r, r') (\gamma - \delta \mu_{\mathcal{X}}(\mathbf{x}'))$$

$$+ k_{\mathcal{X}}(\mathbf{x}, \mathbf{x}') [1 - \delta(\kappa(r) + \kappa(r') - \delta \kappa(r + r'))].$$

For  $\delta = 0$ , we recover the additive model of Eq. 1, while for  $\delta = 1$ , we have that  $f(\mathbf{x}, r) = \gamma$  as  $r \rightarrow 0$ , independent of  $\mathbf{x}$ . This model comes with hyperparameters  $\alpha, \beta, \gamma > 0$  and  $\delta \in [0, 1]$ . We provide an empirical analysis of this model in Section 4.1.1.

### 3.2. Decision about Next Configuration

As in synchronous BOHB (Falkner et al., 2018), we employ the GP surrogate model only to choose configurations  $\mathbf{x}$  for new tasks, while stopping or promotion decisions are done as in HB. Compared to standard BO without multiple fidelities, it is much less clear how a myopically optimal decision would look like in this setting. In this paper, we follow BOHB in choosing  $\mathbf{x}$  by optimizing the expected improvement (EI) acquisition function (Shahriari et al., 2016) over the posterior on  $f(\cdot, r_{\text{acq}})$ , where  $r_{\text{acq}}$  is fixed for each decision. We choose  $r_{\text{acq}} \in \mathcal{R}$  as the largest rung for which at least  $L$  metric values have been observed, where  $L$  is typically set to the input dimensionality (i.e. number of hyperparameters). After some initial period,  $r_{\text{acq}}$  eventually converges to  $r_{\text{max}}$ .

This strategy does not take into account that different choices  $\mathbf{x}$  may have different downstream stopping or promotion consequences. Exploring alternatives to BOHB’s heuristic is an important direction for future work.

## 4. Experiments

We will now present empirical evaluations of our proposed method, comparing it to a range of state-of-the-art HPO

algorithms. For synchronous HB and BOHB, we used the `HpBandSter` package provided by Falkner et al. (2018).<sup>2</sup> For all asynchronous techniques we used `AutoGluon`.<sup>3</sup> We are not aware of a publicly available implementation of (Swersky et al., 2014a) (whose complexity is considerable), nor of follow-up work which is why this is omitted from our experiments.

Below, we refer to our new proposed approach as *asynchronous BOHB*, to be distinguished from *synchronous BOHB* of Falkner et al. (2018). Beyond asynchronous scheduling, we also use a single GP surrogate model for data across all resource levels, while synchronous BOHB uses separate KDE models. Surrogate model hyperparameters (e.g. lengthscales or the covariance amplitude) as well as the noise variance are set by optimizing the log marginal likelihood (empirical Bayes), along with a Gamma hyperprior on the noise variance. Both asynchronous HB and BOHB are further specialized to *stopping* and *promotion* variants (see Section 2). For all multi-fidelity methods we use a halving rate of  $\eta = 3$ . All techniques referred below make use of parallel computation: a set of worker nodes runs training jobs as scheduled, publishing metrics after each epoch, while a master node runs the HP optimizer and the scheduling.

We consider hyperparameter tuning for three different neural network architectures: a fully connected neural network for featurized OpenML (Vanschoren et al., 2014) datasets, a convolutional neural network for image classification, and a recurrent neural network for language modelling. A detailed list of all hyperparameters with their corresponding ranges can be found in Appendix C.

### 4.1. Featurized OpenML Datasets

For our first benchmark, we optimize the hyperparameters and architectural choices of a multi-layer perceptron (MLP) on three featurized classification datasets: *letter* (task ID 6), *electricity* (task ID 1869) and *higgs* (task ID 75101), gathered from OpenML (Vanschoren et al., 2014). While better architectures are available for image or natural language applications, MLPs are frequently used for featurized datasets, and are relatively cheap to train even on standard CPU hardware, which in turn allows for more extensive empirical comparisons.

Our MLP consisted of two hidden layers with ReLU activations (Glorot et al., 2011), followed by a softmax output layer on top. We optimized the learning rate of ADAM (Kingma & Ba, 2015), the batch size and, per layer, the dropout rate, number of units and the scale of a uniform distribution for weight initialization, leading to eight

<sup>2</sup><https://github.com/automl/HpBandSter>

<sup>3</sup><https://github.com/awsml/autogluon>

numerical hyperparameters. Further details are given in Appendix C). We exposed the number of epochs as the resource attribute  $r$ , where  $r_{\min} = 1$  and  $r_{\max} = 27$ . Results for each HPO method are averaged over 50 independent runs with different random seeds. Our performance metric after training time  $t$  is the *immediate regret*  $r_t = y_t - y_*$ , where  $y_*$  is the best observed validation error across all methods, runs and time steps on this dataset. Using the regret in place of just the validation error gives a more detailed picture of progress towards the global optimum. Due to space constraints, we only report results on *letter*, all other results are provided in Appendix D. All experiments are run on `m4.xlarge` AWS EC2 instances.

#### 4.1.1. SURROGATE MODELS

We begin by analysing the influence of the choice of kernel and mean function for  $f(x, r)$  on the performance of the stopping and promotion variant of asynchronous BOHB. We compare different variants of the exponential decay model described in Section 3: fixing  $\delta = 0$  as in Swersky et al. (2014b),  $\delta = 1$ , or learning  $\delta$  with the other GP hyperparameters. We use a Matérn  $\frac{5}{2}$  ARD kernel for the  $k_{\mathcal{X}}$  model between configurations  $x$  (Snoek et al., 2012). As an additional baseline, we use a Matérn  $\frac{5}{2}$  ARD kernel and constant mean function on inputs  $(x, r)$ .

In Figure 2 we compare the various types of kernel for different number of workers. With two workers the exponentially decaying kernel improves upon the Matérn kernel, yet the choice of  $\delta$  does not affect performance. Surprisingly, with four or more workers there is virtually no difference between the surrogate models. While model-based decisions clearly matter (asynchronous BOHB outperforms asynchronous HB), the precise model for inter- or extrapolation along  $r$  seems less important then. In the remaining experiments, we use the exponential decay kernel with learned  $\delta$  as the most flexible choice.

#### 4.1.2. ASYNCHRONOUS SCHEDULING VARIANTS

Next, we compare the stopping and promotion variants of asynchronous scheduling (see Section 2), both for HB and BOHB. Immediate regret over wall-clock time on the *letter* dataset is shown in Figure 3, for 2, 4, 8, and 16 workers, respectively. Qualitatively similar results for the other datasets can be found in Appendix D.

Our results indicate that while the two scheduling variants exhibit certain differences both for HB and BOHB, their size is subdominant to the differences of model-based versus random choice of configurations. Our model-based asynchronous BOHB method clearly outperforms asynchronous HB. In order to reduce the computational costs of our experiments, we use the stopping variant of asynchronous HB and BOHB for all remaining experiments.

#### 4.1.3. ASYNCHRONOUS VS SYNCHRONOUS SCHEDULING

In the last set of experiments for this benchmark we compare asynchronous HB and BOHB with their synchronous counterparts. It should be noted that the synchronous implementations of Falkner et al. (2018) contain some complexities not required in our asynchronous approach. Whenever evaluations for a rung are started, if there are more free workers than slots in the rung, left-over workers are used to immediately start the next bracket. This requires a logic associating workers with brackets, and synchronizing them for batches of evaluations within each rung.

Figure 4 shows the results for synchronous and asynchronous HB and BOHB with 2, 4, 8 and 16 workers. As long as few workers are used (*e.g.*, 2 or 4), synchronous and asynchronous methods perform similarly. However, with more workers (*e.g.*, 8 or 16), asynchronous methods approach the optimum significantly faster. This is likely due to synchronization overhead as well as the more rigid synchronous HB schedule.

Moreover, asynchronous BOHB clearly outperforms asynchronous BO (which uses  $r_{\max}$  evaluations only) in terms of speed of convergence to the optimum. However, we assume that given enough budget, asynchronous BO eventually performs as well or maybe even better than multi-fidelity methods. See for example results on *higgs* dataset with 16 workers in Appendix D; this also has been observed before by Falkner et al. (2018).

In Figure 5, we show the scaling of asynchronous BOHB (stopping) across an increasing number of workers. Doubling the number of workers reduces the runtime roughly by a factor of two. For example, if we increase the number of workers from 2 to 4, asynchronous BOHB achieves the same performance after 2000 seconds now in 1000 seconds (indicated by dashed lines in Figure 5).

## 4.2. Language Modelling

Next, we run HPO for an LSTM (Hochreiter & Schmidhuber, 1997), applied to language modelling on the WikiText-2 dataset (Merity et al., 2016). We optimized the initial learning rate of SGD, batch size, dropout rate, gradient clipping range, and decay factor for the learning rate which is applied if the validation error has not improved upon the previous epoch (details are given in Appendix C). The LSTM consisted of two layers with 1500 hidden units each. For the word embeddings, we also used 1500 hidden units and tied them with the output. We used `g4dn.xlarge` AWS EC2 instances for all experiments and set the minimum resource level to  $r_{\min} = 1$  epochs and the maximum resource level  $r_{\max} = 81$  epochs.

Results comparing asynchronous BOHB, HB, BO and syn-

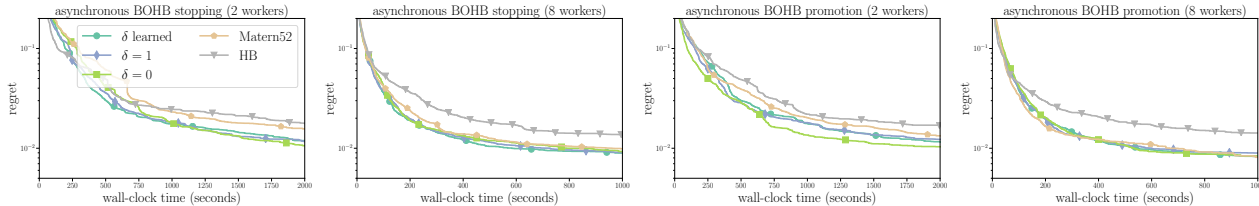


Figure 2. Effect of surrogate model (kernel, mean function) on performance of asynchronous BOHB on *letter* dataset (left: stopping variant; right: promotion variant). We also include HB (random choices) for comparison. With a small number of workers the exponentially decaying kernel improves upon the Matérn baseline, however, with 8 workers there virtually no difference between the different kernels.

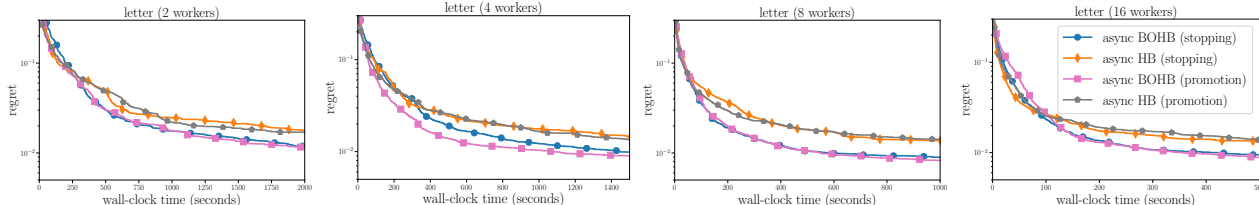


Figure 3. Comparison of promotion and stopping variant for asynchronous HB and BOHB with a variable number of workers. Asynchronous BOHB clearly outperforms asynchronous HB, but there are no significant differences between the promotion and stopping variants.

chronous BOHB using eight workers, are given in Figure 6. Due to the computation cost, we were only able to execute 5 independent runs per method. Asynchronous BOHB outperforms asynchronous HB by halving the wall-clock time to achieve the best performance. Note that, training a LSTM on this dataset for 81 epochs takes roughly 12 hours, which means synchronous BOHB is not able to execute more than a single bracket in the given time budget. Since it requires  $D + 1$  datapoints to fit the KDE, it is not able to fit a model on the highest resource level and therefore performs much worse than asynchronous methods.

### 4.3. Image Classification

Lastly, we consider HPO for the popular wide residual neural network architecture (Zagoruyko & Komodakis, 2016) on the image classification dataset CIFAR-10 (Krizhevsky, 2009). Hyperparameters to be tuned are batch size, weight decay, initial learning rate, momentum and dropout rate (details are given in Appendix C). We split the data into 50000 training and 10000 validation images and applied common data augmentation strategies (cropping and flipping images horizontally with a probability of 0.5). Training is executed by SGD, where the learning rate is adapted by cosine annealing (Loshchilov & Hutter, 2017). We again used the number of epochs as resource and set the minimum resource level to  $r_{\min} = 1$  epochs and the maximum resource level  $r_{\max} = 200$  epochs. As our goal is to compare different HPO methods rather than achieving a new state-of-the-art performance on this benchmark, we did not

apply any further complex regularization techniques which would be required for the latter.

This benchmark is substantially more expensive to run than the MLP experiments above, requiring access to multiple GPUs simultaneously. We therefore compare asynchronous BOHB (our proposed method) to asynchronous HB (stopping variant) and asynchronous BO, average results over 10 repetitions, and use 8 workers. We used `g4dn.xlarge` AWS EC2 instances for this benchmark.

As it can be seen in Figure 7, our new proposed method is able to efficiently exploit low-fidelity signals as well as parallel workers. Not only does it achieve the best final performance overall, it reaches the best final performance of asynchronous HB up to *three hours* earlier.

## 5. Conclusions

We presented a model-based strategy for distributed HPO which combines *asynchronous* Hyperband with Bayesian optimization. To take the current evaluation of pending candidate for the decision-making process into account, we propose a simple but effective joint Gaussian process model across resources and hyperparameter configurations. In contrast, the synchronous state-of-the-art method BOHB uses independent multivariate kernel density estimators for each rung which, compared to our methods, does not allow for fantasizing the outcome of pending candidates. Also, since multivariate kernel density estimators require at least  $D + 1$  observations on the current resource level, synchronous

## Model-based Asynchronous Hyperparameter Optimization

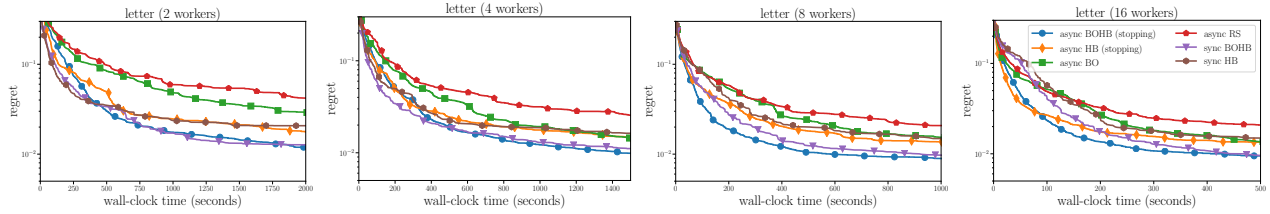


Figure 4. Comparison of different synchronous and asynchronous methods with a variable number of workers. Asynchronous HB and BOHB use the stopping variant. With a small number of workers asynchronous and synchronous BOHB work roughly on par, but if the number of workers increases asynchronous BOHB starts to outperform its synchronous counterpart.

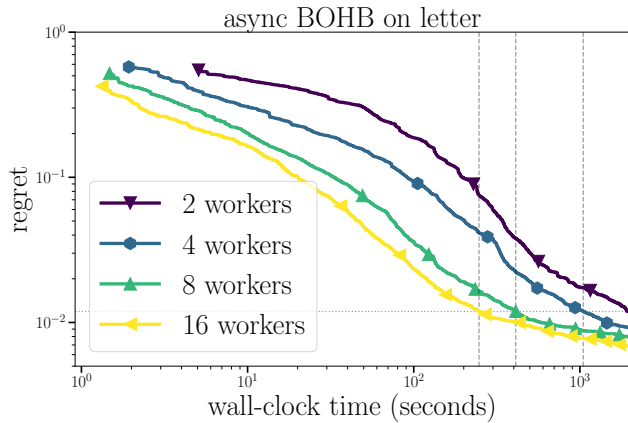


Figure 5. Immediate regret over wall-clock time for asynchronous BOHB with a variable number of workers. Note the log-scale of wall-clock time (different to other plots).

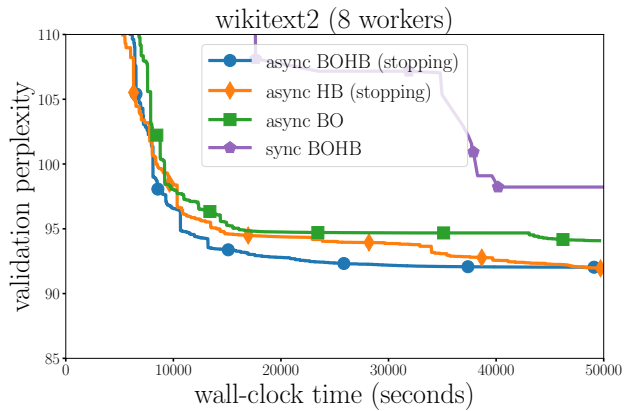


Figure 6. Comparison of asynchronous BOHB with asynchronous Hyperband (HB), each using eight workers for tuning a two-layer LSTM on WikiText-2. Lines are averages over five runs

BOHB requires more data than our method.

In a battery of experiments we show that our new proposed asynchronous BOHB methods outperforms synchronous BOHB and asynchronous HB, especially on very expensive benchmarks. Furthermore, we found that modelling the performance across different rung levels is surprisingly simple and even standard Matérn kernels achieve a reasonable performance. We also compare two version to adapt HB to the asynchronous setting, and found no significant difference when compared on our benchmarks.

In future work, we will explore incorporating our surrogate model for making scheduling decisions based not only on observed, but on predicted outcomes.

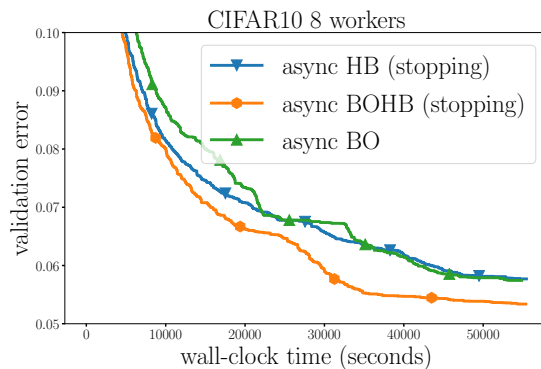


Figure 7. Comparison of asynchronous BOHB with asynchronous Hyperband (HB), each using eight workers for tuning a wide-residual neural network on CIFAR-10. Lines are averages over five runs.



## References

- Alvin, A., Ru, B., Calliess, J. P., Roberts, S., and Osborne, M. A. Asynchronous batch Bayesian optimisation with improved local penalisation. In *Proceedings of the 36th International Conference on Machine Learning (ICML'19)*, 2019.
- Bergstra, J., Bardenet, R., Bengio, Y., and Kegl, B. Algorithms for hyperparameter optimization. In Shawe-Taylor, J., Zemel, R., Bartlett, P., Pereira, F., and Weinberger, K. (eds.), *Advances in Neural Information Processing Systems 24*, pp. 2546–2554. Curran Associates, 2011.
- Cutajar, K., Pullin, M., Damianou, A., Lawrence, N., and González, J. Deep Gaussian processes for multi-fidelity modeling. Technical report, NeurIPS Workshop on Bayesian Deep Learning, 2018.
- Domhan, T., Springenberg, J. T., and Hutter, F. Speeding up automatic hyperparameter optimization of deep neural networks by extrapolation of learning curves. In *Proceedings of the 24th International Joint Conference on Artificial Intelligence (IJCAI'15)*, 2015.
- Falkner, S., Klein, A., and Hutter, F. BOHB: Robust and efficient hyperparameter optimization at scale. In *Proceedings of the 35th International Conference on Machine Learning (ICML 2018)*, 2018.
- Feurer, M. and Hutter, F. Hyperparameter optimization. In Hutter, F., Kotthoff, L., and Vanschoren, J. (eds.), *AutoML: Methods, Systems, Challenges*, chapter 1, pp. 3–37. Springer, 2019.
- Glorot, X., Bordes, A., and Bengio, Y. Deep sparse rectifier neural networks. In Gordon, G. and Dunson, D. (eds.), *Workshop on Artificial Intelligence and Statistics 14*, 2011.
- Hochreiter, S. and Schmidhuber, J. Long short-term memory. *Neural computation*, 1997.
- Jamieson, K. and Talwalkar, A. Non-stochastic best arm identification and hyperparameter optimization. In *Proceedings of the 17th International Conference on Artificial Intelligence and Statistics (AISTATS'16)*, 2016.
- Jones, D., Schonlau, M., and Welch, W. Efficient global optimization of expensive black box functions. *Journal of Global Optimization*, 1998.
- Kandasamy, K., Krishnamurthy, A., Schneider, J., and Poczos, B. Parallelised bayesian optimisation via thompson sampling. In *Proceedings of the 21st International Conference on Artificial Intelligence and Statistics (AISTATS'18)*, 2018.
- Kennedy, M. and O'Hagan, A. Predicting the output from a complex computer code when fast approximations are available. *Biometrika*, 87(1):1–13, 2000.
- Kingma, D. P. and Ba, J. Adam: A method for stochastic optimization. In *International Conference on Learning Representations (ICLR'15)*, 2015.
- Klein, A., Falkner, S., Bartels, S., Hennig, P., and Hutter, F. Fast Bayesian hyperparameter optimization on large datasets. *Electronic Journal of Statistics*, 11, 2017a.
- Klein, A., Falkner, S., Springenberg, J. T., and Hutter, F. Learning curve prediction with Bayesian neural networks. In *International Conference on Learning Representations (ICLR'17)*, 2017b.
- Krizhevsky, A. Learning multiple layers of features from tiny images. Technical report, University of Toronto, 2009.
- Li, L., Jamieson, K., DeSalvo, G., Rostamizadeh, A., and Talwalkar, A. Hyperband: Bandit-based configuration evaluation for hyperparameter optimization. In *International Conference on Learning Representations (ICLR'17)*, 2017.
- Li, L., Jamieson, K., Rostamizadeh, A., Gonina, K., Hardt, M., Recht, B., and Talwalkar, A. Massively parallel hyperparameter tuning. *arXiv:1810.05934 [cs.LG]*, 2018.
- Liaw, R., Liang, E., Nishihara, R., Moritz, P., Gonzalez, J. E., and Stoica, I. Tune: A research platform for distributed model selection and training. *arXiv preprint arXiv:1807.05118*, 2018.
- Loshchilov, I. and Hutter, F. SGDR: Stochastic gradient descent with warm restarts. In *International Conference on Learning Representations (ICLR'17)*, 2017.
- Merity, S., Xiong, C., Bradbury, J., and Socher, R. Pointer sentinel mixture models. *arXiv:1609.07843 [cs.AI]*, 2016.

- Poloczek, M., Wang, J., and Frazier, P. Multi-information source optimization. In Bengio, S., Wallach, H., Larochelle, H., Grauman, K., Cesa-Bianchi, N., and Garnett, R. (eds.), *Advances in Neural Information Processing Systems 31*. Curran Associates, 2018.
- Rasmussen, C. E. and Williams, C. K. I. *Gaussian Processes for Machine Learning*. MIT Press, 2006.
- Shahriari, B., Swersky, K., Wang, Z., Adams, R., and de Freitas, N. Taking the human out of the loop: A review of Bayesian optimization. *Proceedings of the IEEE*, 2016.
- Snoek, J., Larochelle, H., and Adams, R. Practical Bayesian optimization of machine learning algorithms. In Bartlett, P., Pereira, F., Burges, C., Bottou, L., and Weinberger, K. (eds.), *Advances in Neural Information Processing Systems 25*, pp. 2951–2959. Curran Associates, 2012.
- Swersky, K., Snoek, J., and Adams, R. Multi-task Bayesian optimization. In Burges, C., Bottou, L., Welling, M., Ghahramani, Z., and Weinberger, K. (eds.), *Advances in Neural Information Processing Systems 26*. Curran Associates, 2013.
- Swersky, K., Snoek, J., and Adams, R. Freeze-thaw Bayesian optimization. Technical Report arXiv:1406.3896 [stat.ML], ArXiv, 2014a. URL <https://arxiv.org/abs/1406.3896>.
- Swersky, K., Snoek, J., and Adams, R. Freeze-thaw Bayesian optimization. *arXiv:1406.3896 [stat.ML]*, 2014b.
- Valkov, L., Jenatton, R., Winkelmolen, F., and Archambeau, C. A simple transfer-learning extension of hyperband. In *NeurIPS workshop on Meta-Learning 2018*, 2018.
- Vanschoren, J., van Rijn, J., Bischl, B., and Torgo, L. OpenML: Networked science in machine learning. *SIGKDD Explorations*, 2014.
- Zagoruyko, S. and Komodakis, N. Wide residual networks. *arXiv:1605.07146 [cs.CV]*, 2016.

## A. Further Details about Asynchronous Scheduling

Here, we provide some additional details in order to support the main text.

### A.1. Bracket Sampling Distribution

Recall from Section 2 that once a worker is ready to pick up a new task, the corresponding bracket is sampled from a distribution  $P(s)$ . We use

$$P(s) \propto \frac{K+1}{K-s+1} \eta^{K-s}. \quad (3)$$

Note that  $P(s)$  is proportional to the number of configs started in bracket  $s$  in synchronous Hyperband (Li et al., 2017). Focussing on the stopping variant, if the rung size distributions were the same as in synchronous HB (see Appendix A.2), this choice would spend the same amount of aggregate resources in each bracket on average. See Figure 8 for an example.

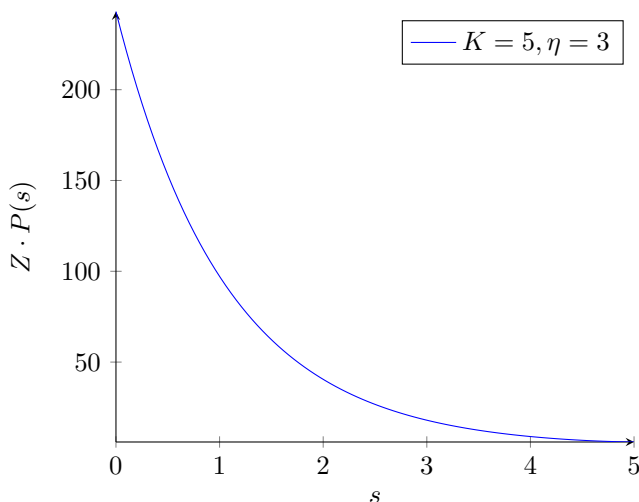


Figure 8. Bracket distribution (unnormalized) for  $K = 5, \eta = 3$ .

### A.2. Controlling Rung Size Ratios

Recall from the end of Section 2 that with asynchronous scheduling (both HB and BOHB), rung size ratios can be skewed away from what is prescribed in synchronous HB and BOHB. Recall that  $c_s[r]$  denotes the (time-variant) number of tasks started in bracket  $s$  to promote a configuration to rung  $r \in B_s$ . In the asynchronous case, we often see  $c_s[r\eta]/c_s[r] > 1/\eta$ , in particular for  $s = 0$  and  $r = r_{\min}$ . We propose a novel option for the promotion variant, where *rung size ratios are controlled*. We track the counts  $c_s[r]$  during the experiment. For any promotion decision at rung  $r$ , we check whether  $c_s[r\eta] \cdot \eta > c_s[r]$ . If so, the result is

“STOP”; otherwise, the normal top  $1/\eta$  condition is evaluated. In other words, we do not allow promotions to rung  $r\eta$  as long as this would skew the size ratio. Our remedy can help to work against the tendency of model-based multi-fidelity HPO to spend too much budget on large resource evaluations.<sup>4</sup>

## B. Further Details about the Model

Here, we provide some additional details in order to support the main text.

### B.1. Posterior Representation. Fantasizing

We employ a standard representation of the Gaussian process posterior (Rasmussen & Williams, 2006). Say that  $k(\mathbf{x}, \mathbf{x}')$  is the kernel function,  $\mu(\mathbf{x})$  the mean function, and the dataset  $\mathcal{D}$  is given by  $\mathbf{X} \in \mathbb{R}^{n \times d}$ ,  $\mathbf{y} \in \mathbb{R}^n$ . For notational simplicity,  $\mathbf{x}$  contains the resource attribute  $r$  here. The representation maintains  $\mathbf{L}$  and  $\mathbf{p}$ , where

$$\mathbf{L}\mathbf{L}^T = \mathbf{K} + \sigma^2 \mathbf{I}_n, \quad \mathbf{p} = \mathbf{L}^{-1}(\mathbf{y} - \mu(\mathbf{X})).$$

Here,  $\mathbf{K} = [k(\mathbf{x}_i, \mathbf{x}_j)] \in \mathbb{R}^{n \times n}$  is the kernel matrix over the training inputs  $\mathbf{X}$ ,  $\sigma^2$  is the noise variance, and  $\mathbf{L}$  is the Cholesky factor (lower triangular, positive diagonal).

Recall that we use *fantasizing* (Snoek et al., 2012) to deal with pending feedback. For  $M$  fantasy samples, we now have a target *matrix*  $\mathbf{Y} \in \mathbb{R}^{n \times M}$ . For any observed configuration  $\mathbf{x}_i$ , the corresponding row in  $\mathbf{Y}$  is  $y_i \mathbf{1}_M^T$ . Now,  $\mathbf{L}$  remains the same, and  $\mathbf{P} = \mathbf{L}^{-1}(\mathbf{Y} - \mu(\mathbf{X}) \mathbf{1}_M^T)$ . Importantly, the dominating computation of  $\mathbf{L}$  is independent of the number  $M$  of fantasy samples. Predictions on test points result in  $M$  different posterior means, but common posterior variances.

In practice, the surrogate model (kernel and mean function) comes with hyperparameters (*e.g.*, noise variance  $\sigma^2$ , length scales and variance of kernel  $k_{\mathcal{X}}$ ,  $\alpha, \beta, \gamma, \delta$ ), which have to be adjusted. We currently use empirical Bayesian optimization (Rasmussen & Williams, 2006) to this end. All in all, recomputing the posterior representation involves (a) optimizing the hyperparameters on the observed dataset only, and (b) drawing fantasy targets, then computing the representation on the extended dataset, including pending configurations. Here, (a) is substantially more expensive than (b), as it involves computing the representation many times during the optimization.

In our implementation of asynchronous HPO, we delay computations of the posterior representation until the next configuration has to be chosen. If running tasks report metric values, they are inserted into the dataset, replacing pending

<sup>4</sup>See the last paragraph of Section 1.4.3 of (Feurer & Hutter, 2019).

configurations entered there before. Our implementation offers a number of strategies to skip the expensive part (a) of the computation. Here, (a) is not skipped initially, until the dataset size passes a threshold. After that, we can skip (a) for all but every  $k$ -th update. Another strategy is to skip (a) as long as the number of *full resource* datapoints ( $\mathbf{x}_i, r_i = r_{\max}$ ) does not grow. This ensures that we do not spend more time on surrogate model updates in the multi-fidelity case than in standard HPO with full resource evaluations only.

## B.2. Derivation of Exponential Decay Surrogate Model

Recall that our novel surrogate model  $k((\mathbf{x}, r), (\mathbf{x}', r'))$  and  $\mu(\mathbf{x}, r)$  is based on the random function assumption (2). Since  $\mathbb{E}[e^{-\lambda r}] = \kappa(r)$ , it is clear that  $\mathbb{E}[f(\mathbf{x}, r)] = \gamma\kappa(r) + \mu_{\mathcal{X}}(\mathbf{x})(1 - \delta\kappa(r)) = \mu_{\mathcal{X}}(\mathbf{x}) + (\gamma - \delta\mu_{\mathcal{X}}(\mathbf{x}))\kappa(r)$ . Moreover,

$$\begin{aligned} k((\mathbf{x}, r), (\mathbf{x}', r')) &= \mathbb{E}[f(\mathbf{x}, r)f(\mathbf{x}', r')] \\ &= (\gamma - \delta\mu_{\mathcal{X}}(\mathbf{x}))\tilde{k}_{\mathcal{R}}(r, r')(\gamma - \delta\mu_{\mathcal{X}}(\mathbf{x}')) + k_{\mathcal{X}}(\mathbf{x}, \mathbf{x}') \\ &\cdot \mathbb{E}\left[(1 - \delta e^{-\lambda r})(1 - \delta e^{-\lambda r'})\right] = (\gamma - \delta\mu_{\mathcal{X}}(\mathbf{x})) \\ &\cdot \tilde{k}_{\mathcal{R}}(r, r')(\gamma - \delta\mu_{\mathcal{X}}(\mathbf{x}')) + k_{\mathcal{X}}(\mathbf{x}, \mathbf{x}') \\ &\cdot (1 - \delta(\kappa(r) + \kappa(r') - \delta\kappa(r + r'))), \\ \tilde{k}_{\mathcal{R}}(r, r') &= \kappa(r + r') - \kappa(r)\kappa(r'). \end{aligned}$$

## B.3. Data for Surrogate Model

What data should be used to fit the surrogate model? Assume that  $r$  is the number of training epochs. If not stopped, we observe  $f(\mathbf{x}, r)$  for  $r = r_{\min}\eta^s, r_{\min}\eta^s + 1, \dots$ , yet only observations at  $r \in B_s$  are taking part in stopping or promotion decisions. In asynchronous BOHB, as detailed in Section 3, we condition the GP model only on observations at rung levels  $r \in r_s$ . Since model computations scale cubically with the data size, this seems sensible to keep costs at bay. Still, our implementation offers two other options. First, as argued in Swersky et al. (2014a), we may use all observed data. However, this drives up the cost for decision-making and might actually more challenging to model of the GP. In this case, we register pending evaluations for  $(\mathbf{x}, r + 1)$  once  $f(\mathbf{x}, r)$  is observed. We also support a third option, which retains observations at  $r \in B_s$ , as well as the most recent  $f(\mathbf{x}, r)$  (i.e., largest  $r$ ). Figure 9 compares the three different options for asynchronous BOHB (stopping) on the letter dataset with 4 workers. The experimental setup is the same as described in Section 4 in the main text. Fitting the GP on all the data indeed lowers the overall performance of BOHB. On the other hand, there is no difference between the first and the third option.

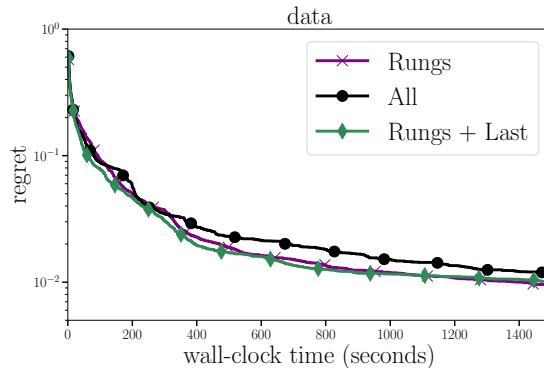


Figure 9. The figure shows the effect of what data is fit to the surrogate model, where ‘Rungs’ means we only used the data at specific rung levels (as done in all experiments in the main paper), for ‘rungs and last’ we additionally feed the last observed value of each learning curve to the GP, and ‘all’ means we fit our model on metric data obtained at all resource levels.

Table 1. The hyperparameters and architecture choices for the fully connected networks.

Hyperparameter	Range
learning rate	$[10^{-6}, 1]$
batch size	$[2^3, 2^7]$
dropout layer 1	$[0, .99]$
dropout layer 2	$[0, .99]$
units layer 1	$[2^4, 2^{10}]$
units layer 2	$[2^4, 2^{10}]$
scale layer 1	$[10^{-3}, 10]$
scale layer 2	$[10^{-3}, 10]$

## C. Configuration Spaces

Table 1 shows the configuration space for the MLP benchmark, Table 2 for the wide residual network benchmark and Table 3 for the LSTM benchmark. If we use an exponential notation than we optimized the corresponding hyperparameter on a logarithmic scale. All hyperparameter were encoded as numerical values.

## D. All Results

In this section we report the result of the MLP benchmark (see Section 4.1 in the main paper) for all three OpenML dataset. Figure 10 shows the results of the average immediate regret with wall-clock time on the x-axis and Figure 11 with the number of epochs on the x-axis. Note that, the Hp-Bandster framework which we used for synchronous BOHB and HB does not store the number of epochs which is why omitted both methods from Figure 11. For an analysis of the result we refer to Section 4.1 in the main paper.

## Model-based Asynchronous Hyperparameter Optimization

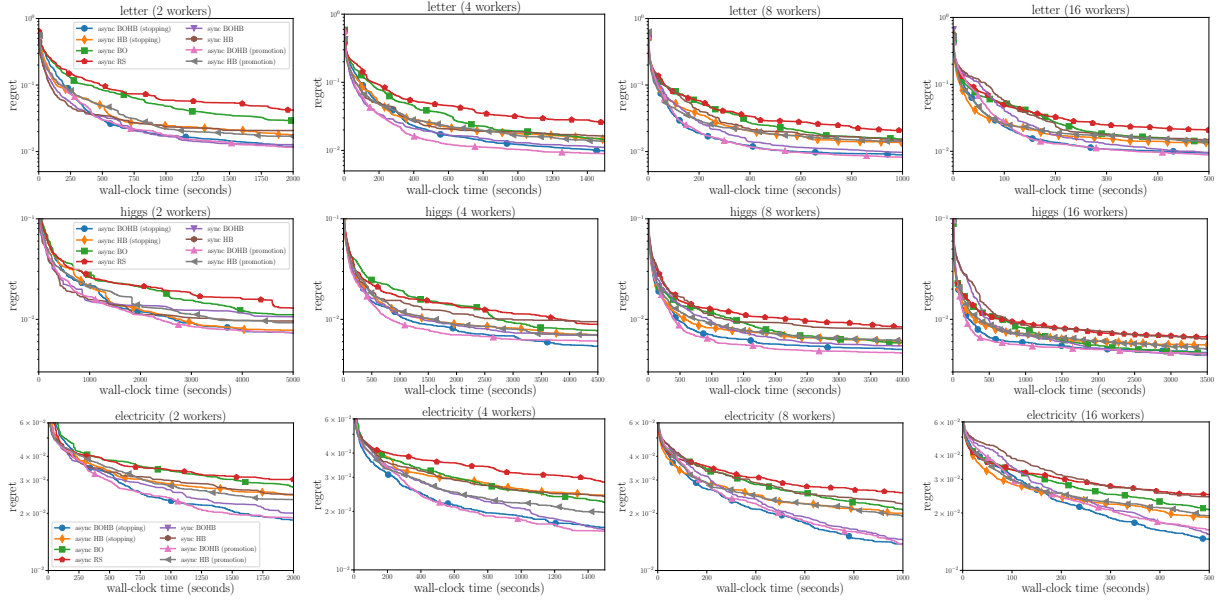


Figure 10. Comparison of all methods on the MLP benchmark over wall-clock time. Each row corresponds to a different dataset and the columns show different number of workers.

Table 2. The configuration space for the wide residual neural network benchmark.

Hyperparameter	Range
initial learning rate	$[5^{-3}, 5^{-1}]$
batch size	$[2^4, 2^7]$
weight decay	$[10^{-5}, 10^{-3}]$
momentum	$[1^{-5}, .99]$
dropout	$[0, .99]$

Table 3. The configuration space for the LSTM benchmark.

Hyperparameter	Range
learning rate	$[1, 50]$
batch size	$[2^3, 2^7]$
dropout	$[0, 0.99]$
gradient clipping	$[0.1, 2]$
learning rate factor	$[1, 100]$

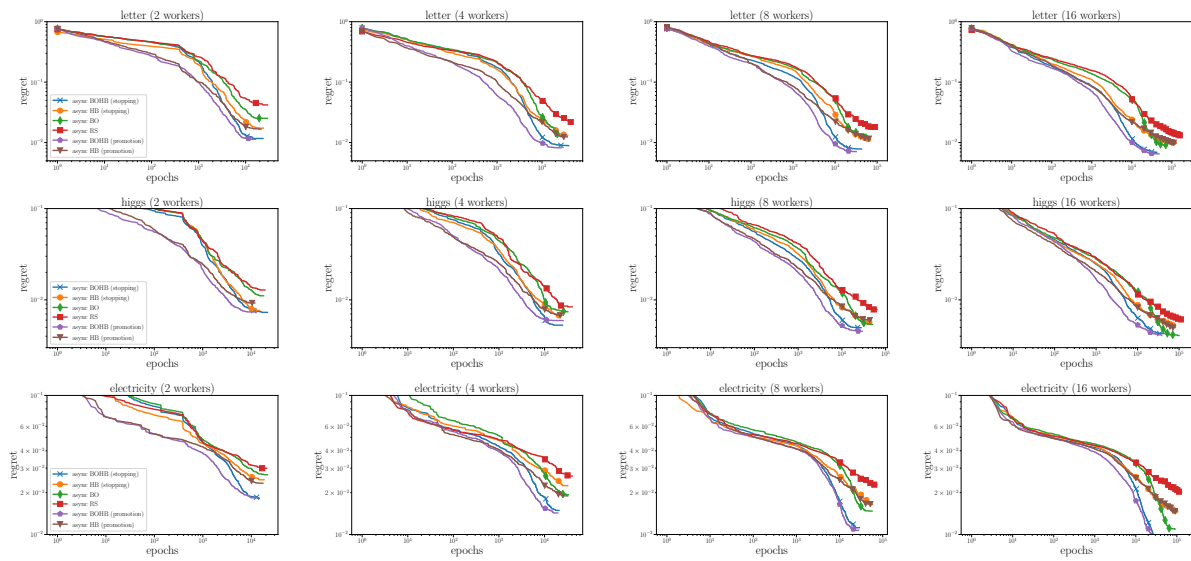


Figure 11. Comparison of all methods on the MLP benchmark over the number of epochs. Each row corresponds to a different dataset and the columns show different number of workers.